

COOCO - Common Objects Out-of-Context - Semantic Violation in Scenes: Investigating Multimodal Context in Referential Communication

Filippo Merlo^{1,2}, Ece Takmaz¹, Wenkai Chen¹, Albert Gatt¹

¹Utrecht University ²University of Trento

f.merlo.research@gmail.com, e.k.takmaz@uu.nl

w.chen5@students.uu.nl, a.gatt@uu.nl

Abstract

Natural scenes provide us with rich contexts for object recognition and reference. In particular, knowing what type of scene one is looking at generates expectations about which objects will occur, and what their spatial configuration should be. Do Vision-Language Models (VLMs) learn to rely on scene contexts in a similar way, when generating references to objects? To address this question, we introduce the *Common Objects Out-of-Context (COOCO)* dataset and test to what extent VLMs rely on scene context to refer to objects under different degrees of scene-object congruency, and different perturbations. Our findings show that models leverage scene context adaptively, depending on both the semantic relatedness between object and scene and the level of noise. In particular, models rely more on context under high target-scene congruence or when objects are degraded. Attention analysis reveals that successful object categorisation involves increased focus on the target in mid-level layers, especially under moderate noise, suggesting that VLMs dynamically balance local and contextual information for reference generation. We make our dataset, code and models available at <https://github.com/cs-nlp-uu/scenereg>.

1 Introduction

Objects rarely appear in isolation. Over time, humans build expectations of seeing certain objects in certain contexts. For instance, we expect to see a laptop on a desk in an office, but not a large piece of ham (Figure 1). Studies of human perception in visual scenes (Vö, 2021; Torralba et al., 2006; Coco et al., 2016) suggest that scenes exhibit both semantic and syntactic regularities (Biederman et al., 1982; Vö, 2021). Violations of either or both of these result in processing difficulties (Ganis and Kutas, 2003; Öhlschläger and Vö,

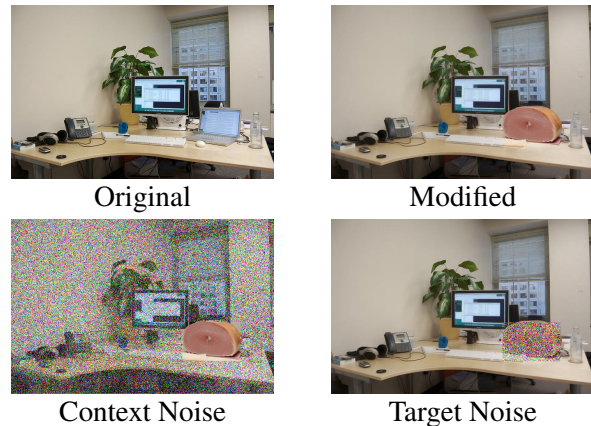


Figure 1: An original image of an office scene from the COCO dataset and *modified* version from our dataset, in which the laptop is replaced with an object that has low relevance to the scene. Bottom: versions of the modified image with Gaussian noise mask (level = 0.5) on the context and on the target.

2016; Vö, 2021).

In this work, we are interested in how Vision-Language Models (VLMs) behave in the presence of *semantic* violations in visual scenes when referring to objects. Such an analysis offers insights into the extent to which models learn to leverage contextual visual information. We focus on **object naming**, that is, the task of determining the category of an object, a fundamental part of Referring Expression Generation (REG; Kraemer and Van Deemter, 2012). The literature on scene perception suggests that scene semantics mediates human viewers' expectations about the objects in a scene, and viewers deploy their attentional resources accordingly. Scene semantics also influence how humans *describe* objects in scenes (Hwang et al., 2011; de Groot et al., 2017, 2015). Do VLMs similarly utilise scene-level visual information when generating descriptions of objects? To study this, we compare the naming

of objects in semantically (in)congruent scenes. If scene-level information guides model choices, then there should be systematic differences between these two conditions in the way models refer to target referents. Previous work has shown the facilitating effects of context in REG, even in the case of perturbations made on images (Junker and Zarrieß, 2024). However, this work does not control for the impact of semantic (in)congruity, and relies on small-scale, purposely-trained models or on artificial images (Junker and Zarrieß, 2025).

We develop a new dataset, Common Objects Out-of-Context (**COOCO**), which manipulates natural images to introduce objects of varying degrees of consistency with the scene (Figure 1). Similarly to Junker and Zarrieß (2024), we further manipulate the visibility of the target referent by introducing different degrees of noise. We summarise the contributions of our study as follows.

1. We present COOCO, a novel dataset to evaluate multimodal models’ capabilities for integrating object-level and scene-level visual information, under both congruent and incongruent conditions.
2. We investigate the impact of scene context on object identification in state-of-the-art VLMs. We show that under conditions where target objects violate scene semantics, scene context acts as a distractor, while it has a clear facilitating effect when the target is congruent with the scene. This also makes models resilient to noise when it is applied to the target region.
3. We investigate how attention is distributed by VLMs across scene components under different conditions of visual semantic congruency, when generating referring expressions.

2 Related Work

Context in Referring Expression Generation. Referring Expression Generation (REG) is the task of generating identifying descriptions for a target object. Early REG approaches relying on handcrafted algorithms (Krahmer and Van Deemter, 2012) incorporated contextual influences by considering the properties that distinguish a target referent from its distractors, with some research also incorporating constraints to guide coherent categorisation for references to plurals, and the use of landmarks for spatial expressions (Schüz et al., 2023). More recent neural

models for *visual REG* learn mappings from raw perceptual inputs to linguistic expressions. Here too there has been limited attention on the ability of models to leverage global scene information (Schüz et al., 2023). This gap has motivated recent investigations into how scene information may enhance robustness in challenging settings (Schüz and Zarrieß, 2023; Junker and Zarrieß, 2025). In particular, Junker and Zarrieß (2024) show that models rely on scene context to generate references even when the target object is fully occluded, indicating that scene context serves not only as a disambiguating constraint but also as a supportive resource for robust reference generation.

Context in Human Object Recognition. Human object recognition is strongly influenced by contextual expectations (Bar, 2004; Oliva and Torralba, 2007; Võ, 2021; Peelen et al., 2023), including both global scene properties (e.g., gist, layout) and local cues (e.g., anchor objects, co-occurring items) (Lauer et al., 2018, 2021; Boettcher et al., 2018). Evidence that visual search is semantically constrained comes from viewing tasks, where viewers fixate more on semantically informative (but not necessarily visually salient) regions, and semantic similarity is a strong predictor of gaze trajectories. Both highly expected and highly incongruent objects attract more attention than moderately fitting ones (Damiano et al., 2024).

Datasets. Widely used vision and language datasets for referring expression and image caption generation, such as COCO (Lin et al., 2015), RefCOCO (Kazemzadeh et al., 2014; Yu et al., 2016a) and VisualGenome (Krishna et al., 2016), lack annotations for object-scene relatedness and do not enable research on semantic violations in scenes. A number of scene violation datasets have been created within the vision community. Prominent examples include ObjAct (Shir et al., 2021), Event Task (Dresang et al., 2019), Out-of-Context (Bomatter et al., 2021), Cut-and-paste dataset (Yun et al., 2021), and SCEGRAM (Öhlschläger and Võ, 2016). However, these datasets tend to be relatively small-scale and do not incorporate degrees of semantic violation or occlusion. In this work, we present a new, large-scale dataset for semantic violations in visual scenes, building on existing resources such as COCO-Search18 (Chen et al., 2021), THINGSPlus (Hebart et al., 2019;

Stoinski et al., 2023) and SUN (Xiao et al., 2010).

3 Dataset Creation

We introduce the **Common Objects Out-of-Context (COOCO)** dataset. We design this dataset to provide a collection of images where the semantic coherence of a scene is disrupted by the presence of a target object with low, medium or high semantic relatedness to the scene type. COOCO builds upon a framework previously established in the visual perception literature with the SCEGRAM dataset (Öhlschläger and Vö, 2017), scaling it up to meet the needs of NLP and computer vision research through a novel methodology.

Images We begin with the publicly available subset of COCO-Search18 (Chen et al., 2021), which includes bounding boxes for target objects. This dataset excludes images with people or animals, categories which are known to significantly influence visual attention (Clarke et al., 2013; End and Gamer, 2017). Excluding such cues, therefore, avoids confounding factors and enables us to study object-scene semantic relationships. COCO-Search18 further excludes images with targets with multiple object instances, controlling for target size, location, and image aspect ratio. We retained the 2,241 images where the target object is present.

Scene labels For each image, we predict the scene label using a Vision Transformer (ViT)¹ (Dosovitskiy et al., 2021) finetuned on SUN-397 (Xiao et al., 2010). We then reduce the SUN label set (397 labels) to 25 (listed in Appendix A), selected to balance frequency and semantic diversity and reclassified the images with the same model, excluding all but the selected labels. This approach mitigates risks of category under-representation and excessive variance. This step provided a scene label for each image.

Object-scene congruency We developed an inpainting pipeline to create versions of images where the target object is replaced with alternatives of varying congruence with the scene (low and medium). We also retain the original image, and additionally include controls where (a) the target is replaced with an object has high relatedness to the scene, and (b) the target is replaced with an

object of the same category as the original. The latter are included to verify if the effects found in the experiments are due to artefacts caused by inpainting in general, or due to the introduction of incongruent object types. Figure 2 shows an example of a scene and its corresponding variants in COOCO.

New objects are determined using human-generated norms in THINGSplus (Stoinski et al., 2023), which includes typicality ratings (the degree of representativeness of an object for higher-level categories) and ratings of the real-world size of objects. We retain only typical objects (typicality ranging from 0.3 to 1) and remove animate objects to ensure consistency with COCO-Search18. We then match COCO-Search18 targets to candidate object types in THINGSPlus with similar real-world size norms. Candidates differing in size from the targets by more than 25 units are excluded.

Our approach to computing semantic relatedness between candidate replacements and scene labels follows Hayes and Henderson (2021), who found strong correlations between embeddings in ConceptNet Numberbatch (Speer et al., 2018) and human visual attention shifts. We use the cosine similarity between scene and object labels to filter low-, medium- and high-similarity candidates.

Image modification Given an image, a scene label and a target object with its bounding region and segmentation-based mask obtained from COCO-Search18 we remove the target from the image, and generate 15 new versions of the scene where the target is replaced with objects having low, medium or high-similarity to the scene label (see Figure 2). We also generate an image containing the target as in the original image as a control condition. Only images that pass a verification test are retained. Full details of the inpainting pipeline and verification tests are in Appendix A.

Final dataset The final COOCO dataset comprises 18,395 images: 1,862 original images with corresponding object-removed versions, 5,480 generated images with low relatedness, 5,572 with medium relatedness, 1,771 with high relatedness, and 1,848 images for the same-target condition.

4 Experimental Setup

We design our experiments to address key research questions concerning how VLMs leverage con-

¹<https://huggingface.co/google/vit-base-patch16-224>



Figure 2: A set of *COOCO* images from the "cubicle office" scene category with target object *laptop*. The target is removed from the original image ('clean') and replaced with objects of the same type ('generated'), as well as targets with high-, low- and medium relatedness to the scene.

textual information for object naming, an essential component of Referring Expression Generation. In particular, we evaluate the extent to which these models rely on scene context when faced with varying degrees of semantic congruence between an object and its background; and on how robustly they perform REG under different levels and configurations of visual noise. With respect to the second of these questions, we address the findings of [Junker and Zarri  \(2024\)](#) more systematically, using a carefully designed dataset and testing a range of state-of-the-art pretrained VLMs.

To achieve this, each model is provided with an image and a specified target region, and is prompted to describe the object within that area using a structured text prompt.

4.1 Models

We use the following models in our experiments: **KOSMOS-2** ([Peng et al., 2024](#)) (1.6B) incorporates mechanisms to establish direct associations between textual spans and specific image regions. It is trained on the GrIT (Grounded Image-Text pairs) web-scale dataset.

Molmo ([Deitke et al., 2024](#)) (7B) is trained on a diverse dataset including ca. 2.3M human-annotated pairs of questions and references to image regions based on 2D points, from 428k images.

xGen-MM-Phi3/BLIP-3 ([Xue et al., 2024](#)) (ca. 4.4B) is trained on the BLIP3-GROUNDING-50M dataset and supports spatial encoding using bounding box coordinates, descriptive spatial re-

lations and/or relative positioning.

LLaVA-OneVision ([Li et al., 2025](#)) (0.5B and 7B) was trained on data with bounding boxes, incorporating RefCOCO ([Kazemzadeh et al., 2014](#); [Yu et al., 2016b](#)) [$>50k$ samples] and Visual Genome ([Krishna et al., 2016](#)) [86k] for single-image settings, and multi-image datasets including WebQA ([Chang et al., 2022](#)) [9.3k]. The model is instruction-tuned to accept spatial information directly in text input in the form of normalised bounding box coordinates.

Qwen2.5-VL ([Bai et al., 2025](#)) (7B) is trained with coordinates based on images' native resolution for grounding, detection, pointing and object counting. The model accepts absolute coordinates for image regions as part of its prompt.

For detailed descriptions of preprocessing steps and region-of-interest (ROI) prompt formats for each model, refer to Appendix B.

Prompts. We test models with structured prompts (details in Appendix B), which include an explicit reference to a region, for example:

What is the object in this part of the image $[x_1, y_1, x_2, y_2]$? Answer with the object's name only. No extra text.

4.2 Noise injection.

We add Gaussian noise ($\lambda = 0.0, 0.5, 1.0$), ranging from mild distortion to complete information loss, to the target region, the context region or the entire image ('All noise'). Pixel values in the affected area are perturbed with noise sampled from

a normal distribution and clipped to stay within valid image ranges.

4.3 Metrics

We evaluate models using three metrics:

RefCLIPScore (Hessel et al., 2022) is the harmonic mean between (1) the CLIPScore (Hessel et al., 2022), which captures the semantic alignment between the generated caption and the image; and (2) the highest cosine similarity between the CLIP (Radford et al., 2021) embeddings of the generated caption and any reference caption.

Text-Based Semantic Similarity, in terms of cosine similarity between CLIP text embeddings, which directly assesses the semantic closeness between the model’s output and the target referent label, as well as between the model’s output and the scene label.

Accuracy, defined as 1 if the cosine similarity between CLIP text embeddings of the model’s output and the target label exceeds a threshold (0.9), and 0 otherwise.²

5 Results

In this section, we report and discuss the main results across all models and experimental conditions in COOCO. We subsequently turn (Sections 6 and 7) to an in-depth exploration of LLaVA-OneVision, which is one of the best-performing models.

Models are sensitive to scene semantics when referring to targets. Figure 3 presents the RefCLIPScore results for each model at noise level 0 across all relatedness conditions. Models achieve the highest scores in the *original* and *same target* conditions, indicating better alignment with the reference when the target object is preserved or replaced by one from the same category. Interestingly, performance is higher in the same target condition than in the original. In contrast, performance declines in conditions where the target object differs from the original (*high*, *medium*, and *low* relatedness). Among these, models perform best in the high relatedness condition, with scores dropping as relatedness decreases. For models depicted in warm colours (the first four), the low re-

²We also computed a hard accuracy metric based on Levenshtein similarity, which quantifies the character-level edit distance between generated and reference captions. Since results are very similar to those obtained with the cosine-based metric, we do not report them here.

latedness condition yields performance that is similar to, or slightly higher than, the medium condition. Conversely, models in cool colours (XGen-MM-Phi3 and Kosmos-2) show a clear and consistent decline in performance with decreasing relatedness.

Scene context acts as a distractor for targets that violate scene semantics. Figure 4a presents RefCLIPScore values aggregated across all models and organized by relatedness categories, noise areas, and noise levels. As expected, models perform best in the zero-noise condition, followed closely by the context noise conditions (noise levels 0.5 and 1 applied outside the target). Similar conclusions can be drawn from the accuracy results (Figure 4b), where the highest accuracy (~ 0.8) is observed in the *original* and *same target* conditions under zero noise and context noise (0.5 and 1.0). These are followed by the high relatedness condition (accuracy ~ 0.5), and the medium and low conditions (accuracy ~ 0.4). Interestingly, in conditions where the target is not related to the scene (medium and low relatedness), the addition of context noise slightly improves performance on RefCLIPScore (Figure 4a), suggesting that target objects that deviate from the scene semantics are better predicted when misleading contextual cues are reduced.

Scene context acts as a facilitator when congruent targets are obscured. In contrast, applying noise directly to the target patch results in a clear performance degradation, proportional to the noise intensity: the higher the noise level, the greater the drop. When noise (at 0.5) is applied to the target or the entire image, accuracy in the original and same target conditions drops to 0.5, while all other conditions approach zero (Figure 4b). For RefCLIPScore, we find that at 0.5 noise level, for the *high*, *medium*, and especially *low* relatedness conditions, performance is more robust when noise is applied to the entire image rather than solely to the target patch. At a higher noise level (1.0), performance continues to decline. However, models perform best with target-specific noise in the *original* and *same target* conditions. This suggests that given a non-perturbed scene context, model predictions for noised target regions are for objects that would be expected given the scene composition. Comparing the 0.5 and 1.0 all-noise settings, we see a sharper drop

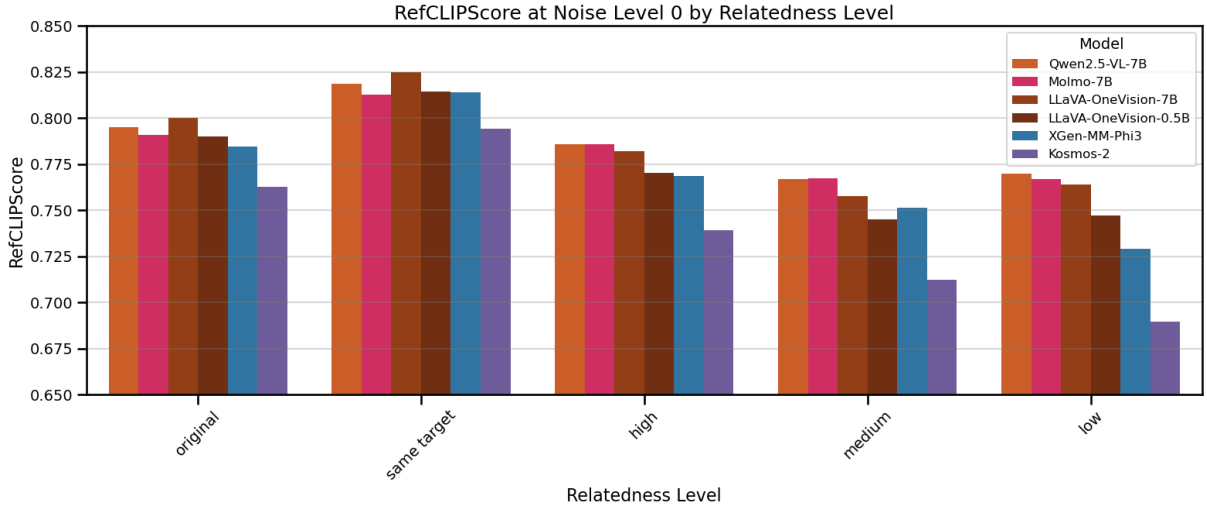
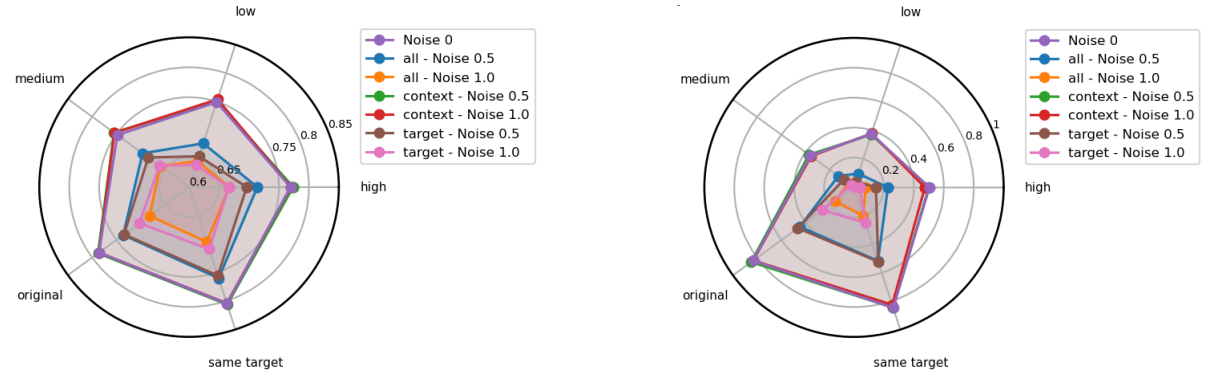


Figure 3: RefCLIPScores per model at noise level 0 across relatedness conditions. Models perform best in the original and same target conditions, with performance declining as target relatedness decreases. Warm-colored models show irregular trends, while cool-colored models exhibit a consistent drop.



(a) RefCLIPScores by relatedness, noise area, and noise level.

(b) Accuracy across noise levels, noise areas, and relatedness conditions.

Figure 4: RefCLIPScore and Accuracy across experimental conditions, aggregated over all models.

for the original and same-target conditions, while the drop is smaller for the high, medium and especially the low relatedness conditions.

6 Output vs. Scene Similarity

We follow up our analysis of overall results with an in-depth focus on one of the models, LLaVA-OneVision-0.5B. As shown in Figure 3, this model performs competitively. Its relatively small size also makes it feasible to analyse in more depth.

We begin in this section with an analysis of the semantic similarity between the model’s predicted reference to the target (e.g. *laptop*), and the scene label for an image (e.g. *office*), to evaluate whether the generation was more strongly anchored to the overall scene or to the target object itself. The results, shown in Figure 5, are separated by accu-

racy, into correct (blue bars) and incorrect (orange bars) responses.

A general trend emerges among both correct and incorrect outputs, namely that when relatedness is medium or low, the model predicts targets which are less semantically related to the scene label. This indicates that the model’s predictions in these conditions are less anchored by the scene semantics. Crucially, when noise is applied to the target region, this trend disappears for incorrect outputs. Notably, across all relatedness conditions involving target noise, correct responses show higher similarity to the scene compared to the no-noise condition. This confirms an observation in Section 5, namely, that when the target is degraded by noise, the model relies more on global scene context. In successful cases, this shift results

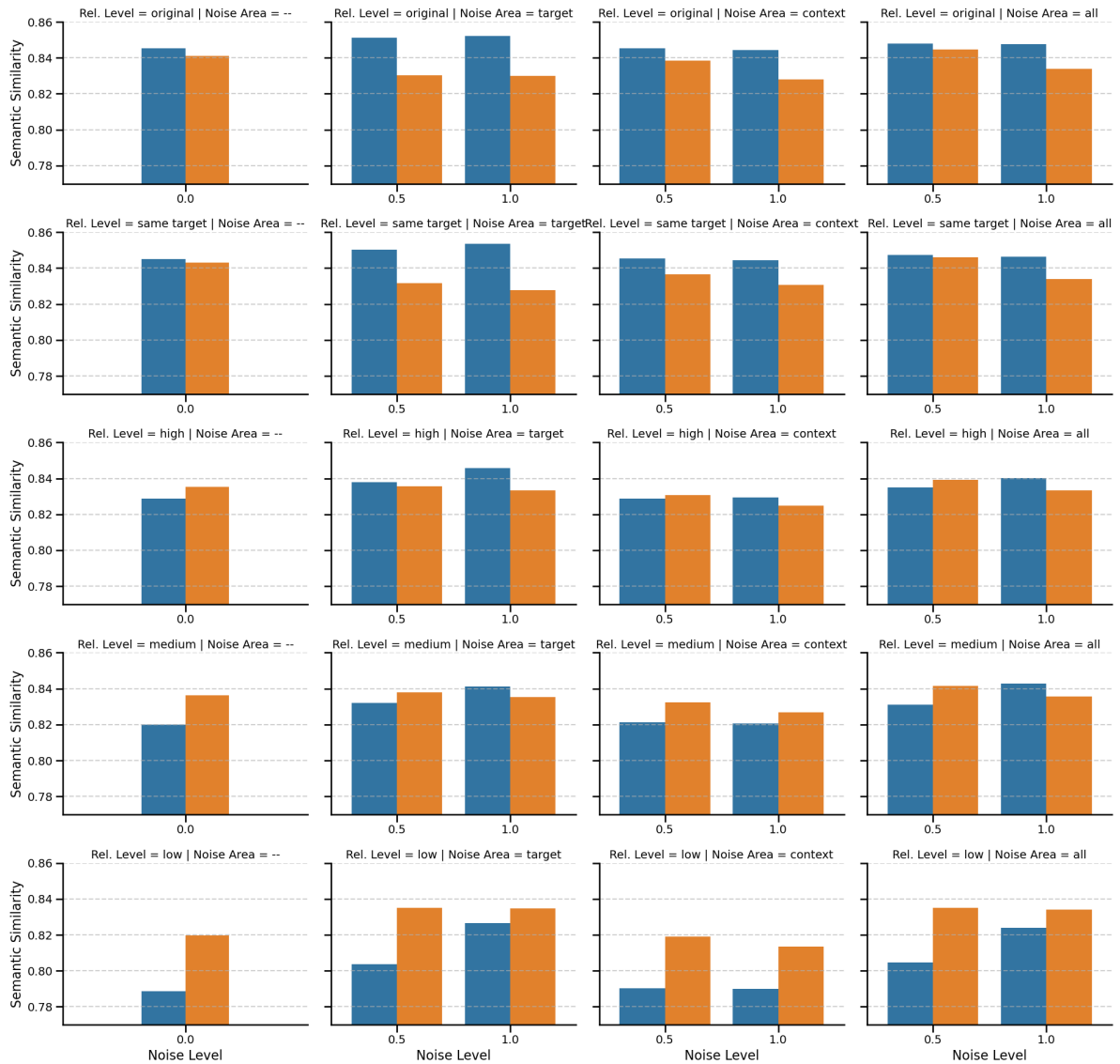


Figure 5: Semantic similarity between outputs and scene labels for the LLaVA-One-Vision 0.5B model. These results are divided by correctness (blue: correct, orange: incorrect), relatedness, noise area, and noise level.

	Original images			Low relatedness		
	Coef.	Std.Err.	z	Coef.	Std.Err.	z
Intercept	1.639	0.044	37.538*	1.598	0.034	46.716*
Noise: Context	-0.006	0.007	-0.787	-0.183	0.004	-41.733*
Noise: Target	-0.048	0.007	-7.364*	-0.032	0.004	-8.042*
Noise level (cont.)	-0.068	0.007	-10.377*	-0.004	0.004	-1.062
Noise level \times Noise: Context	0.051	0.009	5.472*	-0.016	0.006	-2.867*
Noise level \times Noise: Target	0.039	0.007	5.364*	0.066	0.004	14.865*
Group Var	0.047	0.048		0.029	0.029	

Table 1: Linear mixed effects model: Noise area and noise level on scene-target semantic similarity, for original and low relatedness contexts. * denotes a significant effect at $p \leq .01$. Conditional R^2 values: 0.52 (original) and 0.39 (low rel.)

in outputs that are more semantically aligned with the scene.

We further analyse these results using a Linear Mixed Effects (LME) analysis, with semantic sim-

ilarity between predicted target and scene label as the dependent variable. We include noise level (modeled as a continuous variable, scaled and centered) and noise area (comparing target and context noise conditions to the ‘all’ noise condition) as predictors, with random intercepts for scene labels.³ For this analysis, we do not separate correct and incorrect outputs, focusing instead on the similarity of the model’s prediction to the scene in the two conditions representing the ‘extreme’ cases of target-scene congruence, namely, the original and the low-relatedness conditions.

Table 1 summarises the LME results. The most important observations are related to the interactions between noise level and noised region: for original images, as noise increases in both the target region and the context region, there is a marginal increase in the semantic similarity of the predicted target to the scene label. For images in the low relatedness condition, increasing noise in the context region results in a significant decrease in similarity between model predictions and scene label.

7 Attention Deployment Analysis

Maintaining our focus on the 0.5B version of LLaVA-OneVision (Li et al., 2025), we now turn to an analysis of the model’s attention dynamics under different experimental conditions.

To analyze attention allocation across different layers l of the vision encoder and COOCO samples t , we compute the ratio r between the total normalized attention values assigned to the target (a_{target}) and the context (a_{context}): $r_l^{(t)} = \frac{a_{\text{target},l}^{(t)}}{a_{\text{context},l}^{(t)}}$. A value of r closer to 1 indicates a higher allocation of attention to the target region, whereas a value closer to 0 suggests greater attention to the context. Since the context area is larger than the target, we do not expect r to exceed 0.5. Instead, our focus is on analyzing its variations across different experimental conditions. We then compute the mean ratio value for each encoder layer by averaging across all samples: $\bar{r}_l = \frac{1}{T} \sum_{t=1}^T r_l^{(t)}$ where T denotes the total number of instances. This allows us to assess how attention is distributed across different hierarchical levels of the encoder under varying experimental conditions.

³We do not include a full random effects structure, as introducing random slopes resulted in poor convergence.

Full details of how we extract attention values and compute layerwise attention ratios are in Appendix C.

Targets that violate scene semantics attract more attention.

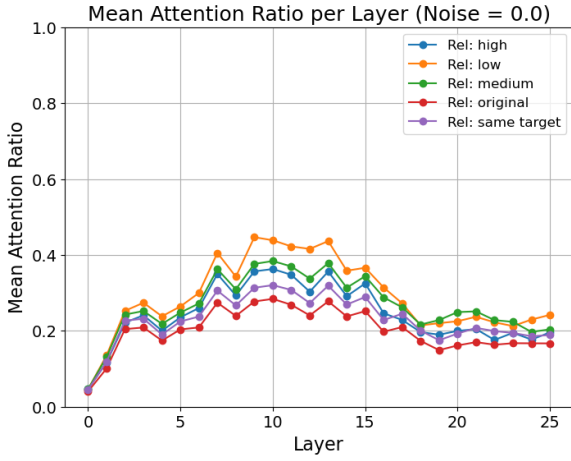
Figure 6 shows the attention allocation ratio across layers \bar{r}_l for different semantic relatedness conditions at zero noise, separated by correct and incorrect responses according to the accuracy metric (Section 4.3). First, we observe that, for correct responses, the model generally applies more attention to the target compared to incorrect ones. Second, target-focused attention is primarily concentrated in the middle layers, peaking between layers 7 and 15. Third, the model’s attention to the target is clearly modulated by its semantic relatedness to the scene: more attention is allocated in the *low-relatedness* condition, followed by the *medium-relatedness* condition, and lowest in the *high-relatedness* condition. The least attention is allocated to the target in the *original* condition, while the *same target* condition receives slightly more. Interestingly, this pattern of increased attention to less semantically related targets also appears in incorrect responses. This suggests that even when the model fails to correctly name the object, it may still detect its incongruity with the surrounding scene, allocating more attention to targets that appear out of place.

Targets attract attention even under moderate noise conditions.

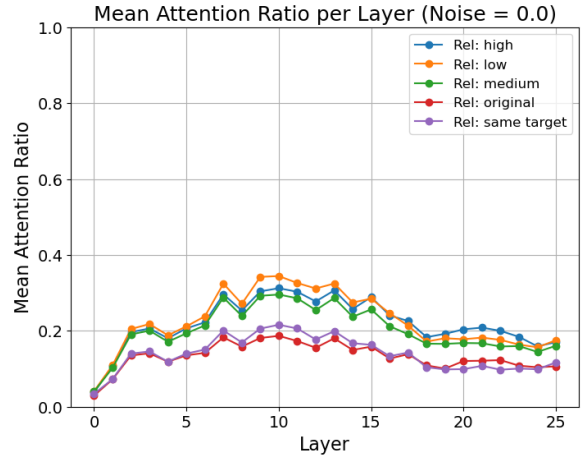
Figure 7 compares mean attention-to-target ratio \bar{r}_l heatmaps for correct versus incorrect model responses across the three noise levels (0.0, 0.5, 1.0) and three perturbation conditions (All Input, Context only, Target only). The analysis shows that moderate noise on the target (e.g., noise level 0.5 in the All Input and Target Only conditions) tends to increase attention to the target in correct responses particularly in the middle layers (7-14), suggesting that the model compensates for partial degradation by focusing more on the target. However, when the noise becomes too severe, attention to the target declines, likely because the target information becomes less recoverable. In contrast, under the Context Only condition, higher noise levels consistently lead to increased attention on the target, indicating a re-allocation of focus away from the noisy context toward the unaltered target.

Higher attention to the target is linked to correct responses under noisy conditions.

Fig-

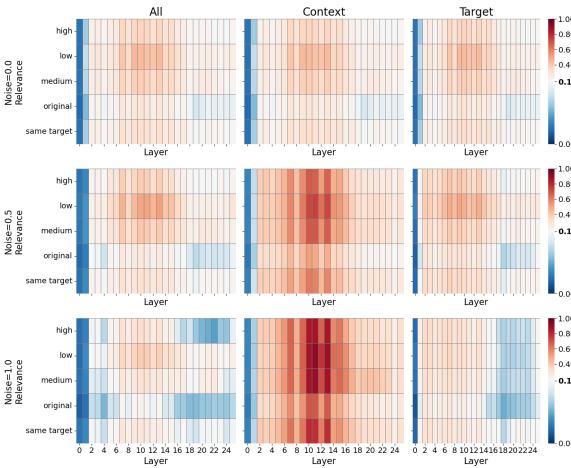


Correct Responses

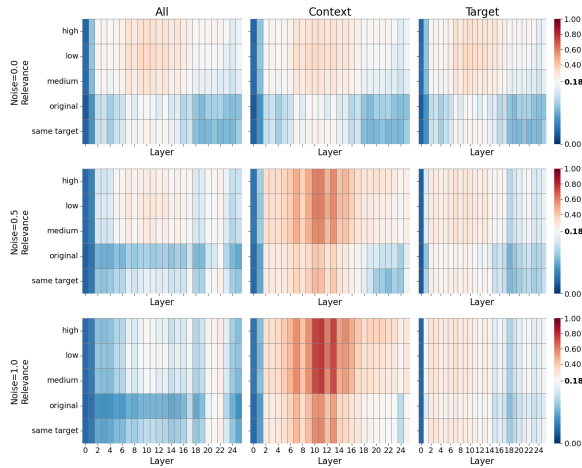


Incorrect Responses

Figure 6: Layer-wise attention allocation ratio on the target object across semantic relatedness conditions at zero noise, split by correct and incorrect responses.



Correct Responses



Incorrect Responses

Figure 7: Layer-wise attention heatmaps showing how the model’s focus on the target varies with noise level (rows: none, moderate, high) and noise location (columns: full input, context only, target only). Warmer colors indicate stronger attention relative to the no-noise baseline (average attention ratio ~ 0.18), while cooler colors indicate reduced attention.

Figure 8 visualises the change in mean attention-to-target ratio $\Delta \bar{r}_l$ between correct and incorrect responses, across all experimental conditions. The heatmaps are predominantly green, indicating that when the model correctly recognizes the object, it tends to allocate more attention to the target token compared to when it misclassifies the object. This effect becomes more pronounced under higher noise conditions, particularly in the middle layers of the transformer (7-14). However, this observation is affected by both noise and target-scene relatedness: when a medium (0.5) level of noise is

applied to the target or the whole image, correct object categorisation is marked by notably higher attention to the target, compared to incorrect cases.

8 Discussion

Several patterns emerge from our experimental findings. Firstly, the RefCLIPScore analysis reveals that models consistently exhibit superior performance when either the original target object or a semantically similar one is present. This may be due to the COCO images having been included in the training data of all models. However, the

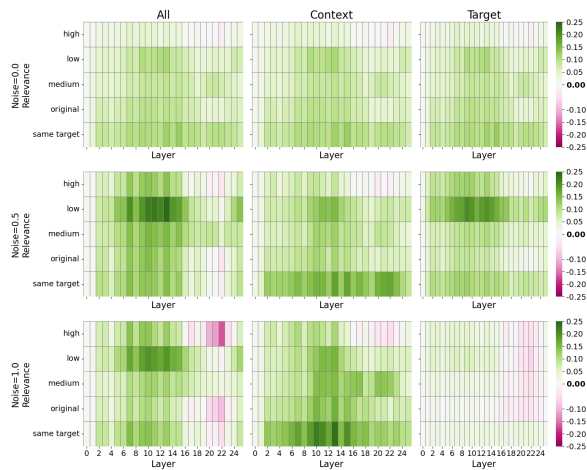


Figure 8: Difference in mean attention-to-target ratio ($\Delta\bar{r}_l$) between correct and incorrect model predictions across layers, per noise level. Green shades indicate higher attention in correct responses compared to incorrect ones, while pink shades indicate the opposite. The diverging colour map is centered at zero and scaled symmetrically to ± 0.25 , the maximum observed delta.

observation that scores are slightly higher for the "same target" condition compared to the "original" condition suggests that models benefit from slight semantic shifts within the same category, perhaps because categorising an object similar but not identical to the original introduces nuanced semantic cues that models leverage e.g., the generated same-category object is more prototypical than the actual object, making it easier to classify for the model. Moreover, the drop in performance corresponding to decreasing relatedness shows how sensitive models are to object semantics. The accuracy data aligns well with RefCLIP-Score patterns, emphasising the robustness of object categorisation in zero- and context-noise conditions. However, target-specific noise substantially diminishes performance, emphasising the models' reliance on clear object representations.

The output versus scene similarity results for the LLaVA-One-Vision model indicate that as semantic relatedness diminishes, models tend to anchor outputs more to the semantics of the target rather than the broader scene. When target objects are corrupted by noise, correct responses shift towards a stronger reliance on scene context, implying an adaptive strategy that leverages global context to compensate for degraded local features.

In attention analysis, clear differences emerge

in attention allocation. Correct categorisation consistently involves higher attention on the target, particularly in middle layers (7–15), suggesting critical semantic processing occurs there, as already pointed out by previous multimodal interpretability studies on the LLaVA model family (Zhang et al., 2025a,b; Golovanevsky et al., 2025). A compelling observation is the inverse relationship between semantic relatedness and attention allocation: less scene-related targets receive more focused attention. Furthermore, noise conditions modulate attention dynamics significantly. Moderate target-specific noise (0.5 level) appears to trigger a compensatory increase in target-focused attention, aiding correct recognition. Conversely, extreme noise (level 1.0) forces models to shift reliance entirely to context. This dynamic attention behaviour highlights an adaptive mechanism within the models, balancing local target analysis against global context integration depending on image clarity and semantic coherence.

Overall, these findings suggest that vision-language models dynamically modulate their semantic and attentional strategies, demonstrating adaptability that hinges heavily on target clarity and semantic coherence with the visual scene. This suggests that models become sensitive to scene semantics during training.

9 Conclusion

Repeated exposure to common visual scenes generates expectations about what objects are likely to occur (the 'semantics' of the scene; Vö, 2021). In this paper, we address whether state-of-the-art multimodal models acquire such knowledge in the course of training. Experiments on COOCO, a novel dataset which carefully controls for the target-scene congruence, reveals that scene semantics play an important role in the way in which models generate references to objects, though the extent to which models rely on scene context versus the target region itself is modulated by perturbations to these image regions. Our findings are consistent with recent work on simple, artificial scenes, which suggest that VLMs leverage scene context (Junker and Zarriß, 2024, 2025). Our analysis of attention is also consistent with findings from a growing body of interpretability research, which suggests that middle layers of VLMs play a crucial role in cross-modal fusion (Zhang et al., 2025a,b; Golovanevsky et al., 2025).

Acknowledgements

This research was supported by the Netherlands Science Foundation (NWO) under the AiNed AiNed XS Europe 2023, grant number NGF.1609.23.020. FM was a visiting student from the University of Trento to Utrecht University during the period when the work was conducted. We thank Sina Zarri , Simeon Junker and Hendrik Buschmeier for their valuable comments and helpful discussions.

References

- Shuai Bai, Keqin Chen, Xuejing Liu, Jialin Wang, Wenbin Ge, Siboz Song, Kai Dang, Peng Wang, Shijie Wang, Jun Tang, Humen Zhong, Yuanzhi Zhu, Mingkun Yang, Zhaohai Li, Jianqiang Wan, Pengfei Wang, Wei Ding, Zheren Fu, Yiheng Xu, Jiabo Ye, Xi Zhang, Tianbao Xie, Zesen Cheng, Hang Zhang, Zhibo Yang, Haiyang Xu, and Junyang Lin. 2025. [Qwen2.5-VL Technical Report](#). ArXiv:2502.13923 [cs].
- Moshe Bar. 2004. [Visual objects in context](#). *Nature Reviews Neuroscience*, 5(8):617–629.
- Irving Biederman, Robert J. Mezzanotte, and Jan C. Rabinowitz. 1982. [Scene perception: Detecting and judging objects undergoing relational violations](#). *Cognitive Psychology*, 14(2):143–177.
- Sage E. P. Boettcher, Dejan Draschkow, Eric Dierker, and Melissa L.-H. V . 2018. [Anchoring visual search in scenes: Assessing the role of anchor objects on eye movements during visual search](#). *Journal of Vision*, 18(13):11.
- Philipp Bomatter, Mengmi Zhang, Dimitar Kerev, Spandan Madan, Claire Tseng, and Gabriel Kreiman. 2021. [When Pigs Fly: Contextual Reasoning in Synthetic and Natural Scenes](#). ArXiv:2104.02215 [cs].
- Yingshan Chang, Mridu Narang, Hisami Suzuki, Guihong Cao, Jianfeng Gao, and Yonatan Bisk. 2022. [WebQA: Multihop and Multimodal QA](#). ArXiv:2109.00590 [cs].
- Yupei Chen, Zhibo Yang, Seoyoung Ahn, Dimitris Samaras, Minh Hoai, and Gregory Zelinsky. 2021. [COCO-Search18 fixation dataset for predicting goal-directed attention control](#). *Scientific Reports*, 11(1):8776.
- Alasdair D F Clarke, Moreno I. Coco, and Frank Keller. 2013. [The impact of attentional, linguistic, and visual features during object naming](#). *Frontiers in Psychology*, 4(DEC):1–12.
- Moreno I. Coco, Frank Keller, and George L. Malcolm. 2016. [Anticipation in real-world scenes: The role of visual context and visual memory](#). *Cognitive Science*, 40(8):1995–2024.
- Claudia Damiano, Maarten Leemans, and Johan Wagemans. 2024. [Exploring the Semantic-Inconsistency Effect in Scenes Using a Continuous Measure of Linguistic-Semantic Similarity](#). *Psychological Science*, 35(6):623–634.
- Matt Deitke, Christopher Clark, Sangho Lee, Rohun Tripathi, Yue Yang, Jae Sung Park, Mohammadreza Salehi, Niklas Muennighoff, Kyle Lo, Luca Soldaini, Jiasen Lu, Taira Anderson, Erin Bransom, Kiana Ehsani, Huong Ngo, Yensung Chen, Ajay Patel, Mark Yatskar, Chris Callison-Burch, Andrew Head, Rose Hendrix, Favyen Bastani, Eli VanderBilt, Nathan Lambert, Yvonne Chou, Arnavi Chheda, Jenna Sparks, Sam Skjonsberg, Michael Schmitz, Aaron Sarnat, Byron Bischoff, Pete Walsh, Chris Newell, Piper Wolters, Tanmay Gupta, Kuo-Hao Zeng, Jon Borchardt, Dirk Groeneveld, Crystal Nam, Sophie Lebrecht, Caitlin Wittlif, Carissa Schoenick, Oscar Michel, Ranjay Krishna, Luca Weihs, Noah A. Smith, Hananeh Hajishirzi, Ross Girshick, Ali Farhadi, and Aniruddha Kembhavi. 2024. [Molmo and pixmo: Open weights and open data for state-of-the-art vision-language models](#).
- Alexey Dosovitskiy, Lucas Beyer, Alexander Kolesnikov, Dirk Weissenborn, Xiaohua Zhai, Thomas Unterthiner, Mostafa Dehghani, Matthias Minderer, Georg Heigold, Sylvain Gelly, Jakob Uszkoreit, and Neil Houlsby. 2021. [An Image is Worth 16x16 Words: Transformers for Image Recognition at Scale](#). ArXiv:2010.11929 [cs].
- Haley C. Dresang, Michael Walsh Dickey, and Tessa C. Warren. 2019. [Semantic memory for objects, actions, and events: A novel test of event-related conceptual semantic knowledge](#). *Cognitive Neuropsychology*, 36(7-8):313–335.

- Albert End and Matthias Gamer. 2017. Preferential processing of social features and their interplay with physical saliency in complex naturalistic scenes. *Frontiers in Psychology*, 8(March):418.
- Giorgio Ganis and Marta Kutas. 2003. An electrophysiological study of scene effects on object identification. *Cognitive Brain Research*, 16(2):123–144.
- Michal Golovanevsky, William Rudman, Vedant Palit, Carsten Eickhoff, and Ritambhara Singh. 2025. What Do VLMs NOTICE? A Mechanistic Interpretability Pipeline for Gaussian-Noise-free Text-Image Corruption and Evaluation. In *Proceedings of the 2025 Conference of the Nations of the Americas Chapter of the Association for Computational Linguistics: Human Language Technologies (Volume 1: Long Papers)*, pages 11462–11482, Albuquerque, New Mexico. Association for Computational Linguistics.
- Floor de Groot, Falk Huettig, and Christian N. L. Olivers. 2015. When Meaning Matters: The Temporal Dynamics of Semantic Influences on Visual Attention. *Journal of Experimental Psychology: Human Perception and Performance*.
- Floor de Groot, Falk Huettig, and Christian N.L. Olivers. 2017. Language-induced visual and semantic biases in visual search are subject to task requirements. *Visual Cognition*, 0(0):1–16. Publisher: Taylor & Francis.
- Taylor R. Hayes and John M. Henderson. 2021. Looking for semantic similarity: What a vector-space model of semantics can tell us about attention in real-world scenes. *Psychological Science*, 32(8):1262–1270. PMID: 34252325.
- Martin N. Hebart, Adam H. Dickter, Alexis Kidder, Wan Y. Kwok, Anna Corriveau, Caitlin Van Wicklin, and Chris I. Baker. 2019. THINGS: A database of 1,854 object concepts and more than 26,000 naturalistic object images. *PLOS ONE*, 14(10):e0223792.
- Jack Hessel, Ari Holtzman, Maxwell Forbes, Roman Le Bras, and Yejin Choi. 2022. CLIPScore: A Reference-free Evaluation Metric for Image Captioning. ArXiv:2104.08718.
- Alex D. Hwang, Hsueh-Cheng Wang, and Marc Pomplun. 2011. Semantic guidance of eye movements in real-world scenes. *Vision Research*, 51(10):1192–1205. Publisher: Elsevier Ltd.
- Benoit Jacob, Skirmantas Kligys, Bo Chen, Menglong Zhu, Matthew Tang, Andrew Howard, Hartwig Adam, and Dmitry Kalenichenko. 2017. Quantization and Training of Neural Networks for Efficient Integer-Arithmetic-Only Inference. ArXiv:1712.05877 [cs].
- Simeon Junker and Sina Zarrieß. 2024. Resilience through scene context in visual referring expression generation. In *Proceedings of the 17th International Natural Language Generation Conference*, pages 344–357, Tokyo, Japan. Association for Computational Linguistics.
- Simeon Junker and Sina Zarrieß. 2024. Resilience through Scene Context in Visual Referring Expression Generation. ArXiv:2404.12289 [cs].
- Simeon Junker and Sina Zarrieß. 2025. Scene-gram: Conceptualizing and Describing Tangrams in Scene Context. *arXiv preprint arXiv:2506.11631*.
- Sahar Kazemzadeh, Vicente Ordonez, Mark Maten, and Tamara Berg. 2014. ReferItGame: Referring to Objects in Photographs of Natural Scenes. In *Proceedings of the 2014 Conference on Empirical Methods in Natural Language Processing (EMNLP)*, pages 787–798, Doha, Qatar. Association for Computational Linguistics.
- Emiel Kraemer and Kees Van Deemter. 2012. Computational Generation of Referring Expressions: A Survey. *Computational Linguistics*, 38(1):173–218.
- Ranjay Krishna, Yuke Zhu, Oliver Groth, Justin Johnson, Kenji Hata, Joshua Kravitz, Stephanie Chen, Yannis Kalantidis, Li-Jia Li, David A. Shamma, Michael S. Bernstein, and Fei-Fei Li. 2016. Visual Genome: Connecting Language and Vision Using Crowdsourced Dense Image Annotations. ArXiv:1602.07332 [cs].
- Tim Lauer, Tim H. W. Cornelissen, Dejan Draschkow, Verena Willenbockel, and Melissa L.-H. Võ. 2018. The role of scene summary statistics in object recognition. *Scientific Reports*, 8(1):14666.

- Tim Lauer, Filipp Schmidt, and Melissa L.-H. Võ. 2021. [The role of contextual materials in object recognition](#). *Scientific Reports*, 11(1):21988.
- Bo Li, Yuanhan Zhang, Dong Guo, Renrui Zhang, Feng Li, Hao Zhang, Kaichen Zhang, Peiyuan Zhang, Yanwei Li, Ziwei Liu, and Chunyuan Li. 2025. [LLaVA-onevision: Easy visual task transfer](#). *Transactions on Machine Learning Research*.
- Tsung-Yi Lin, Michael Maire, Serge Belongie, Lubomir Bourdev, Ross Girshick, James Hays, Pietro Perona, Deva Ramanan, C. Lawrence Zitnick, and Piotr Dollár. 2015. [Microsoft COCO: Common Objects in Context](#). ArXiv:1405.0312 [cs].
- Haotian Liu, Chunyuan Li, Qingyang Wu, and Yong Jae Lee. 2023. [Visual Instruction Tuning](#). ArXiv:2304.08485 [cs].
- Sabine Öhlschläger and Melissa L.-H. Võ. 2016. [Scegram: An image database for semantic and syntactic inconsistencies in scenes](#). *Behavior Research Methods*, 49:1780 – 1791.
- Aude Oliva and Antonio Torralba. 2007. [The role of context in object recognition](#). *Trends in Cognitive Sciences*, 11(12):520–527.
- Marius V. Peelen, Eva Berlot, and Floris P. De Lange. 2023. [Predictive processing of scenes and objects](#). *Nature Reviews Psychology*, 3(1):13–26.
- Zhiliang Peng, Wenhui Wang, Li Dong, Yaru Hao, Shaohan Huang, Shuming Ma, Qixiang Ye, and Furu Wei. 2024. [Grounding multimodal large language models to the world](#). In *The Twelfth International Conference on Learning Representations*.
- Alec Radford, Jong Wook Kim, Chris Hallacy, Aditya Ramesh, Gabriel Goh, Sandhini Agarwal, Girish Sastry, Amanda Askell, Pamela Mishkin, Jack Clark, Gretchen Krueger, and Ilya Sutskever. 2021. [Learning Transferable Visual Models From Natural Language Supervision](#). ArXiv:2103.00020 [cs].
- Simeon Schüz, Albert Gatt, and Sina Zarrieß. 2023. [Rethinking symbolic and visual context in Referring Expression Generation](#). *Frontiers in Artificial Intelligence*, 6:1067125.
- Simeon Schüz and Sina Zarrieß. 2023. [Keeping an Eye on Context: Attention Allocation over Input Partitions in Referring Expression Generation](#). In *Proceedings of the Workshop on Multimodal, Multilingual Natural Language Generation and Multilingual WebNLG Challenge (MM-NLG 2023)*, pages 20–27, Prague, Czech Republic. Association for Computational Linguistics.
- Yarden Shir, Naphtali Abudarham, and Liad Mudrik. 2021. [You won’t believe what this guy is doing with the potato: The ObjAct stimulus-set depicting human actions on congruent and incongruent objects](#). *Behavior Research Methods*, 53(5):1895–1909.
- Robyn Speer, Joshua Chin, and Catherine Havasi. 2018. [ConceptNet 5.5: An Open Multilingual Graph of General Knowledge](#). ArXiv:1612.03975 [cs].
- Laura M. Stoinski, Jonas Perkuhn, and Martin N. Hebart. 2023. [THINGSplus: New norms and metadata for the THINGS database of 1854 object concepts and 26,107 natural object images](#). *Behavior Research Methods*.
- Roman Suvorov, Elizaveta Logacheva, Anton Mashikhin, Anastasia Remizova, Arsenii Ashukha, Aleksei Silvestrov, Naejin Kong, Harshith Goka, Kiwoong Park, and Victor Lempitsky. 2021. [Resolution-robust Large Mask Inpainting with Fourier Convolutions](#). ArXiv:2109.07161 [cs].
- Antonio Torralba, Aude Oliva, Monica S. Castelhano, and John M. Henderson. 2006. [Contextual guidance of eye movements and attention in real-world scenes: The role of global features in object search](#). *Psychological Review*, 113(4):766–786.
- Jesse Vig and Yonatan Belinkov. 2019. [Analyzing the Structure of Attention in a Transformer Language Model](#). In *Proceedings of the 2019 ACL Workshop BlackboxNLP: Analyzing and Interpreting Neural Networks for NLP*, pages 63–76, Florence, Italy. Association for Computational Linguistics.
- Melissa Le-Hoa Võ. 2021. [The meaning and structure of scenes](#). *Vision Research*, 181:10–20.

- Jianxiong Xiao, James Hays, Krista A. Ehinger, Aude Oliva, and Antonio Torralba. 2010. [SUN database: Large-scale scene recognition from abbey to zoo](#). In *2010 IEEE Computer Society Conference on Computer Vision and Pattern Recognition*, pages 3485–3492, San Francisco, CA, USA. IEEE.
- Le Xue, Manli Shu, Anas Awadalla, Jun Wang, An Yan, Senthil Purushwalkam, Honglu Zhou, Viraj Prabhu, Yutong Dai, Michael S Ryoo, Shrikant Kendre, Jieyu Zhang, Can Qin, Shu Zhang, Chia-Chih Chen, Ning Yu, Juntao Tan, Tulika Manoj Awalgaoonkar, Shelby Heinecke, Huan Wang, Yejin Choi, Ludwig Schmidt, Zeyuan Chen, Silvio Savarese, Juan Carlos Niebles, Caiming Xiong, and Ran Xu. 2024. [xgen-mm \(blip-3\): A family of open large multimodal models](#).
- Licheng Yu, Patrick Poirson, Shan Yang, Alexander C. Berg, and Tamara L. Berg. 2016a. [Modeling Context in Referring Expressions](#). ArXiv:1608.00272 [cs].
- Licheng Yu, Patrick Poirson, Shan Yang, Alexander C Berg, and Tamara L Berg. 2016b. [Modeling Context in Referring Expressions](#). In *ECCV*. ArXiv: 1608.00272.
- Woo-han Yun, Taewoo Kim, Jaeyeon Lee, Jaehong Kim, and Junmo Kim. 2021. [Cut-and-Paste Dataset Generation for Balancing Domain Gaps in Object Instance Detection](#). *IEEE Access*, 9:14319–14329. ArXiv:1909.11972 [cs].
- Xiaohua Zhai, Basil Mustafa, Alexander Kolesnikov, and Lucas Beyer. 2023. [Sigmoid Loss for Language Image Pre-Training](#). ArXiv:2303.15343 [cs].
- Jiarui Zhang, Mahyar Khayatkhoei, Prateek Chhikara, and Filip Ilievski. 2025a. [MLLMs Know Where to Look: Training-free Perception of Small Visual Details with Multimodal LLMs](#). ArXiv:2502.17422 [cs].
- Zhi Zhang, Srishti Yadav, Fengze Han, and Ekaterina Shutova. 2025b. [Cross-modal Information Flow in Multimodal Large Language Models](#). ArXiv:2411.18620 [cs].
- Junhao Zhuang, Yanhong Zeng, Wenran Liu, Chun Yuan, and Kai Chen. 2024. [A Task is Worth One Word: Learning with Task Prompts for High-Quality Versatile Image Inpainting](#). ArXiv:2312.03594 [cs].
- Sabine Öhlschläger and Melissa Le-Hoa Võ. 2017. [SCEGRAM: An image database for semantic and syntactic inconsistencies in scenes](#). *Behavior Research Methods*, 49(5):1780–1791.

A Further details on COOCO image creation

living room, arrival gate outdoor, restaurant, market/outdoor, parking lot, bakery shop, arrival gate/outdoor, art studio, gas station, banquet hall, tower, street, music studio, fastfood restaurant, pantry, cubicle/office, market outdoor, kitchen, coffee shop, bedroom, dorm room, cubicle office, delicatessen, train railway, bakery/shop, home office, physics laboratory, dining room, bathroom

Table 2: The 25 scene labels in the COOCO dataset

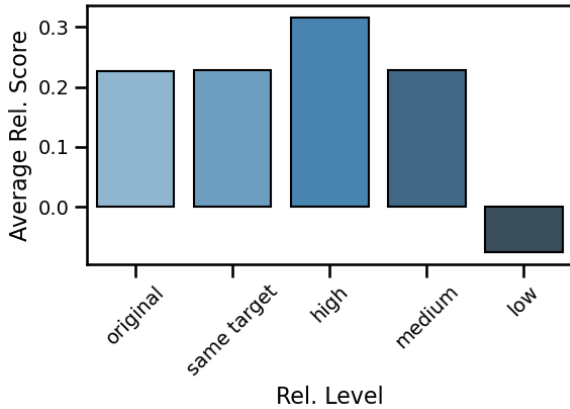


Figure 9: Average relatedness scores grouped by relatedness level, illustrating the semantic similarity between scenes and candidate objects.

A.1 Description of the inpainting and verification pipeline

For inpainting, we use the LaMa inpainting model (Suvorov et al., 2021) to remove the target object from a scene, expanding its mask by 20% to make sure that the resulting image is free of irregularities. We then create a square-padded version of the cleaned image, and create a mask for object inpainting,

For each of the three relatedness groups (low, medium, and high), we retain 15 replacement candidates. In the high-similarity condition only, the similarity to the original target object is also considered. Additionally, we generate one image containing the same target object as in the original image to use as a control condition. See Figure 9 for the distribution of relatedness scores per relatedness level.

We randomly sample one candidate, and generate a descriptive prompt using the 8-bit quantised (Jacob et al., 2017) LLaVA model (Liu et al., 2023). We perform inpainting using PowerPoint (Zhuang et al., 2024), guiding the inpainting process with the LLaVA-generated descriptive prompt as a positive prompt and a fixed negative prompt to suppress undesired content. We set the fitting degree (which controls how closely the output adheres to the shape of the mask) to 0.6 (0-1), use 45 (0-50) diffusion steps to balance quality and compute efficiency, and apply a guidance scale of 7.5 (0-30) that controls for alignment with the prompt.

We verify resulting images using LLaVA through a binary visual query assessing the presence of the generated candidate object in the image; if rejected, the guidance scale is increased by 7.5, and the process is repeated up to four times until the maximum guidance scale level of 30. If all attempts fail, a new candidate is sampled. This process yields 8 generated images per input (3 each for the low- and medium relatedness conditions, 1 for high relatedness, and 1 for the same-target condition). A second round of filtering is applied using full-precision LLaVA to ensure final quality.

B Spatial Encoding & Model Prompts

KOSMOS-2

KOSMOS-2 employs a discretized token-based representation of spatial information. The key principle is to transform continuous image coordinates into discrete location tokens via a grid-based partitioning of the image space. Each image is divided into a $P \times P$ grid, and every bounding box is encoded by mapping its top-left and bottom-right corners to location tokens. These tokens are then embedded in the textual input using a structured format that mimics hyperlink annotations, explicitly marking visual references within language. This design enables KOSMOS-2 to align and jointly reason over linguistic spans and visual regions in a shared sequence modeling framework.

KOSMOS-2

KOSMOS-2 encodes spatial regions by discretizing bounding boxes into location tokens and embedding them alongside natural language using `<grounding>` tags.

Prompt:

`<grounding>`What is the object in `<phrase>`this part`</phrase>` of the image? Answer with the object's name only. No extra text.
Answer:

xGen-MM

xGen-MM embeds bounding box coordinates within the prompt using `<bbox>` tags and learns to interpret these as visual region references in natural language form.

Prompt:

`<luser!>` `<image>`What is the object in this part `<bbox>`[x1, y1][x2, y2]`</bbox>` of the image? Answer with the object's name only. No extra text.`<lend!>`
`<lassistant!>`

Molmo

Molmo grounds language in visual space using a point-based strategy. Instead of bounding boxes, it represents spatial references as single (x, y) coordinates, normalized to a fixed-scale $[0,100]$ grid. Such grounding enables the model to identify, count, or compare objects based on minimal visual supervision. The model interprets these point references directly from the linguistic input, treating them as spatial queries in the generation process.

Qwen2.5-VL

Qwen2.5-VL builds upon the Qwen-VL architecture by integrating visual tokens into a large language model using enhanced spatial encoding strategies. It employs bounding box references enclosed in square bracket format $[x_1, y_1, x_2, y_2]$, where coordinates are normalized within the range $[0,1]$. The spatial references are directly inserted into the natural language prompt, making them interpretable as explicit multimodal instructions.

Molmo

Molmo grounds text in visual space using single-point references normalized to a $[0,100]$ scale. These coordinates are embedded directly in the natural language prompt.

Prompt:

What is the object at point $x = 63, y = 44$ of the image? Answer with the object's name only. No extra text.

Qwen2.5-VL

Qwen2.5-VL encodes normalized bounding box coordinates directly in the prompt as $[x_1, y_1, x_2, y_2]$, supporting explicit multimodal alignment through instruction-tuned sequences.

Prompt:

What is the object in this part of the image $[x_1, y_1, x_2, y_2]$? Answer with the object's name only. No extra text.

xGen-MM (BLIP-3)

xGen-MM encodes spatial grounding using natural language expressions that describe object locations via bounding box coordinates.

LLaVA-OneVision

LLaVA-OneVision employs a normalized bounding box encoding strategy embedded directly in the textual prompt in the form $[x_1, y_1, x_2, y_2]$, where all values fall within the $[0,1]$ range.

LLaVA-OneVision

LLaVA-OneVision embeds bounding boxes in $[0,1]$ range directly in the prompt, leveraging instruction-tuned pretraining to interpret spatial references as tasks.

Prompt:

What is the object in this part of the image $[x1, y1, x2, y2]$? Answer with the object’s name only. No extra text.

C Attention over image tokens in LLaVA-OneVision

LLaVA-OneVision handles an image–question pair in four stages:

1. Following the AnyRes visual tokenization strategy, the input image is resized and tiled into $a \times b$ crops of the same resolution. Each view – including the full image – is encoded by the SigLIP SO400M ViT (Zhai et al., 2023) into T tokens, yielding $L = (a \times b + 1) T$ tokens in total. If L surpasses the threshold τ , bilinear interpolation reduces the per-crop token count.
2. All visual tokens are projected via a two-layer MLP into the LLM’s embedding space;
3. The resulting image tokens are prepended to the tokenized question together with an answer-start marker;
4. The LLM then decodes the answer autoregressively.

In Section 7, we restrict our analysis to the visual tokens obtained from the fixed encoding of the full image, omitting any multi-crop tokens.

Below, we detail the process of aggregating attention values and computing the layerwise attention allocation ratio $r_l^{(t)}$ described in Section 7.

C.1 Aggregating LLM Attention

We first extract the attention deployed by the LLM decoder over image tokens. Let the attention tensor be $A \in \mathbb{R}^{L \times H \times N \times N}$, where L is the number of layers, H is the number of attention heads, and N is the number of tokens. For each layer l , we compute the mean attention over heads: $\bar{A}_l = \frac{1}{H} \sum_{h=1}^H A_{l,h}$. To improve interpretability,

we follow a common practice of zeroing out attention directed toward the beginning-of-sequence (BOS) token, which often absorbs a disproportionate amount of attention due to its special role in autoregressive models (Vig and Belinkov, 2019). Specifically, for each attention matrix \bar{A}_l , we set the column corresponding to the BOS token to zero, effectively removing all incoming attention to this token. We then normalize each row so that its values sum to one, resulting in a normalized attention matrix $\hat{A}_l \in \mathbb{R}^{N \times N}$.

We aggregate attention across layers to obtain the final LLM attention matrix: $A_{\text{LLM}} = \frac{1}{L} \sum_{l=1}^L \hat{A}_l$. Our method distinguishes between prompt tokens and generated tokens in accordance with the autoregressive nature of the model. Prompt tokens receive attention from all subsequent tokens, while generated tokens attend only to preceding tokens. To construct the attention representation, we first process the prompt tokens by computing their attention matrix as described above.

For generated tokens, we apply a similar procedure with two key modifications: (1) only the last row of each attention matrix is retained, corresponding to the attention from the newly generated token, and (2) attention to the BOS token is nullified as before. Each resulting attention vector is then padded to a common length and stacked with the aggregated prompt token attention matrix.

C.2 Aggregating Attention in Vision Transformers (ViTs)

During our initial experiments, we noticed a tendency where the model applied attention over a specific set of tokens for many images, indicating a model-intrinsic bias. To mitigate such systematic attention biases, we compute a layer-wise average attention map across the dataset and subtract it from each instance’s attention map. This adjustment emphasizes instance-specific patterns by removing model-intrinsic tendencies. To avoid resolution-based confounds, we include only images of size 640×640 (which comprise 86% of the dataset).

Per-Instance Layer Aggregation: For each image instance $t \in T$ and layer $l \in L$, we average the attention across heads: $\bar{A}_l^{(t)} = \frac{1}{H} \sum_{h=1}^H A_{l,h}^{(t)}$. We then normalize each row of $\bar{A}_l^{(t)}$ so that attention values sum to one, yielding a normalized attention map $A_{\text{norm},l}^{(t)}$.

Dataset-Wide Averaging: To capture general attention patterns, we compute the average normalized attention map across all instances: $A_{\text{avg},l} = \frac{1}{T} \sum_{t=1}^T A_{\text{norm},l}^{(t)}$. These maps serve as baselines for interpreting the attention behavior of individual instances. The final per-instance attention map is computed by subtracting the baseline and applying ReLU: $A_{\text{ViT},l}^{(t)} = \text{ReLU} \left(A_{\text{norm},l}^{(t)} - A_{\text{avg},l} \right)$. This operation retains only positive deviations from the dataset-wide mean, highlighting unique attention patterns for each instance. Each column of $A_{\text{ViT},l}^{(t)}$, corresponding to a vision token $j \in J$, is reshaped into a spatial attention map $V_j \in \mathbb{R}^{g \times g}$, where g is the number of image patches per side (e.g., $g = 27$ for SO400M). These maps represent spatial distributions of attention at the selected layer.

C.3 Attention Over Image Regions

To analyze how the model distributes its focus across visual inputs during generation, we compute attention over image regions.

Let $O = \{o_1, o_2, \dots, o_{|O|-1}\}$ denote the set of the LLM decoder output tokens, excluding the final `<|im_end|>` token, which is not semantically informative. For each output token $o_i \in O$, we extract the corresponding attention weights $A_{\text{LLM},i,j}$ from the LLM attention matrix, where j indexes the vision tokens. These attention weights are normalised to yield $\hat{A}_{i,j}$.

Each vision token j is associated with a spatial map $V_j \in \mathbb{R}^{g \times g}$, derived from the adjusted ViT attention described earlier. The attention map over the image for output token o_i is then computed as a weighted sum: $A_i^{\text{img}} = \sum_{j \in J} \hat{A}_{i,j} \cdot V_j$. To obtain a global attention map for the image, we average over all output tokens: $A_{\text{final}}^{\text{img}} = \frac{1}{|O|-1} \sum_{i \in O} A_i^{\text{img}}$. This attention map is then upsampled to the original image resolution using nearest-neighbor interpolation for visualization.

C.4 Attention Over Target and Context

To analyze how attention is distributed between the target object and the surrounding context, we extract the bounding box $B = (x_{\min}, y_{\min}, w, h)$ of the target object region. The total attention over the target area is computed as: $a_{\text{target}} = \sum_{(x,y) \in B} A_{\text{final}}^{\text{img}}(x, y)$. Similarly, the attention over the context region, excluding both the target and irrelevant padding areas, is given by:

$a_{\text{context}} = \sum_{(x,y) \in C} A_{\text{final}}^{\text{img}}(x, y)$, where C represents the pixels outside the target bounding box but within the valid image region.

The entire process is carried out for each layer of the vision backbone model, for each of which we have a specific aggregated attention representation $A_{\text{ViT},l}$, ensuring that we obtain an attention distribution over the image, and thus over both the target and context, specific to each layer.

C.5 Attention Allocation Ratio

To analyze attention allocation across different levels l of the vision encoder and experimental instances t , we compute the ratio r between the total normalized attention values assigned to the target (a_{target}) and the context (a_{context}): $r_l^{(t)} = \frac{a_{\text{target},l}^{(t)}}{a_{\text{context},l}^{(t)}}$. A value of r closer to 1 indicates a higher allocation of attention to the target region, whereas a value closer to 0 suggests greater attention to the context. Since the context area is larger than the target, we do not expect r to exceed 0.5. Instead, our focus is on analyzing its variations across different experimental conditions.

We then compute the mean ratio value for each encoder layer by averaging across all instances: $\bar{r}_l = \frac{1}{T} \sum_{t=1}^T r_l^{(t)}$ where T denotes the total number of instances. This allows us to assess how attention is distributed across different hierarchical levels of the encoder under varying experimental conditions.